Betulinic acid alleviates the inflammatory injury of osteoblasts in osteoporosis by augmenting autophagy via the AMPK-mTOR signaling pathway

YIWEI ZHAO[1*], ZECHAO QU[1*], LIN LIU[2*], YONG ZHANG[1], XIAOHAO WANG[1], BO ZHANG[1], YINING GONG[1] and LIANG YAN[1]

[1]Department of Spine Surgery, Honghui Hospital, Xi'an Jiao Tong University, Xi'an, Shaanxi 710054, P.R. China; [2]Department of Critical Care Medicine, Honghui Hospital, School of Medicine, Xi'an Jiao Tong University, Xi'an, Shaanxi 710054, P.R. China

Received September 1, 2025; Accepted April 16, 2026

DOI: 10.3892/ijmm.2026.5858

Abstract. Osteoporosis (OP) is a systemic disease characterized by a reduction in the number of trabecular bone structures and damage to the bone microstructure. It is commonly found in people who are aging or have estrogen deficiency. Oxidative stress and chronic inflammation caused by pathological factors such as aging and estrogen deficiency are key pathogenic factors. Betulinic acid (BA), a natural pentacyclic triterpenoid compound, exhibits anti-inflammatory and antioxidant biological effects. However, its role and potential mechanisms in the inflammatory injury of osteoblasts in OP remain unclear. In the present study, *in vivo* experiments were conducted using an ovariectomized (OVX) rat model of OP, with bone microstructure analyzed by micro-CT, protein expression detected by immunohistochemistry, and serum inflammatory factors measured by ELISA. BA was revealed to alleviate bone loss in OVX rats and inhibit the expression of NOD-like receptor pyrin domain-containing 3 (NLRP3), Asc and caspase-1 in the femur of OVX rats, as well as suppress the release of inflammatory factors such as interleukin-1 β, interleukin-6, and tumor necrosis factor-αin the serum of rats. The inflammatory injury osteoblast model of BA intervention was also studied with hydrogen peroxide (H_2O_2) *in vitro*, with reactive oxygen species (ROS) levels assessed by fluorescence assay, osteogenic differentiation evaluated by ALP staining and alizarin red staining, and autophagy-related proteins detected by western blotting. BA pretreatment reduced production of ROS, inhibited expression of NLRP3 and downstream pathway activation, improved alkaline phosphatase activity, mineralization ability, and osteogenic differentiation ability of MC3T3-E1 cells. Administration of BA increased the autophagy of MC3T3-E1 cells treated with H_2O_2, which was confirmed by the increased expression levels of LC3b II and Beclin-1 and the decreased expression levels of P62. In addition, BA could enhance the phosphorylation of AMPK in MC3T3-E1 cells treated with H_2O_2 and reduce the phosphorylation of mTOR, but this effect could be rescued by Compound C (an AMPK blocker). BA can protect osteoblasts from inflammatory injury by reducing the production of ROS and inhibiting the activation of NLRP3 through autophagy mediated by the AMPK/mTOR pathway.

Introduction

Osteoporosis (OP), as a common bone metabolism disease, is characterized by decreased bone density and destruction of the bone tissue microstructure. These alterations lead to a significant increase in bone notable and a substantial rise in the probability of fractures. As a result, it severely impairs the patients' quality of life, elevates the mortality rate, and imposes a heavy economic burden. It has already become a global health challenge (1). Currently, in clinical practice, drug-based treatment approaches for OP, such as bisphosphonates and estrogen replacement therapy, are employed. However, these methods have certain side effects and limitations, including issues such as jawbone necrosis, atypical femoral fractures, and increased risk of cardiovascular disease (2-4). Therefore, it is particularly important to explore new treatment methods for OP.

OP is a metabolic disease caused by multiple factors. Its main causes of onset include endocrine factors, genetic and immune factors, nutritional factors, sex and age factors, disease and drug factors, disuse and environmental factors. Among them, the pathophysiology that has received the majority of attention mainly emphasizes the endocrine mechanism, such as estrogen deficiency and aging (5-7). Changes in these factors lead to the body being in a microenvironment of chronic

Correspondence to: Professor Liang Yan, Department of Spine Surgery, Honghui Hospital, Xi'an Jiao Tong University, 555 Youyi East Road, Xi'an, Shaanxi 710054, P.R. China
E-mail: yanliangdr5583@163.com

*Contributed equally

Key words: betulinic acid, autophagy, osteoblasts, AMPK-mTOR signaling, inflammatory

inflammation, ultimately resulting in insufficient osteogenic ability of osteoblasts or enhanced bone resorption by osteoclasts, thereby disrupting normal bone metabolism (8,9). According to a previous study, the levels of interleukin-6 (IL-6), interleukin-1β (IL-1β), and tumor necrosis factor-α (TNF-α) in the serum of ovariectomized (OVX) rats are markedly increased compared with the control group (10). As a key molecule that can induce inflammatory factors IL-6 and TNF-α, nuclear factor-κB (NF-κB) can markedly inhibit the expression levels of osteocalcin (OCN) and runt-related transcription factor 2 (RUNX2) in bone marrow mesenchymal stem cells (BMSCs) when elevated, thereby affecting their osteogenic differentiation ability (11). In addition, hydrogen peroxide (H_2O_2) can activate the NOD-like receptor pyrin domain-containing 3 (NLRP3) inflammasome mediated by NF-κB, which in turn leads to inflammatory injury and pyroptosis of osteoblasts (12). It has been reported that the expression levels of the NLRP3 inflammasome increase in the primary BMSCs of OVX mice, and caspase-1 and IL-1β are activated, which further inhibits osteoblast differentiation (13). Estrogen deficiency or oxidative stress may lead to the activation of the NLRP3 inflammasome in osteoblasts, thus triggering the pathological process of OP.

BA, a natural pentacyclic triterpenoid compound, is mostly extracted from plants such as birch trees. It has attracted extensive attention due to its potent pharmacological effects, including anti-inflammatory, antioxidant and antitumor activities (14,15). Regarding its anti-inflammatory properties, BA exerts anti-inflammatory effects by regulating multiple inflammatory signaling pathways. For example, it can significantly inhibit the activation of the NF-κB signaling pathway, the central hub of inflammatory responses, thereby reducing the transcription and secretion of pro-inflammatory cytokines such as IL-6, TNF-α and IL-1β in inflammatory cells (16). Furthermore, studies have shown that BA can suppress the phosphorylation of p38 mitogen-activated protein kinases (MAPKs), which further blocks inflammatory reactions in pathological microenvironments (17). In terms of antioxidant activity, BA can enhance the activity of endogenous antioxidant enzymes in cells, such as superoxide dismutase and glutathione peroxidase, while reducing the accumulation of reactive oxygen species (ROS) (18,19). This regulation helps mitigate oxidative stress-induced cellular damage and maintain the structural and functional integrity of cell. Research findings suggest that part of the mechanisms underlying the actions of BA can be ascribed to its regulation of autophagy, which verifies that BA serves as a key regulator in autophagy (20,21). In addition, autophagy plays a bridging role in inhibiting the activation of the NLRP3 inflammasome (22-24).

Autophagy, an evolutionarily conserved intracellular degradation process, carries out an indispensable regulatory role in maintaining bone homeostasis (25). For osteoblasts, moderate autophagy can protect them against inflammatory and oxidative stress damage: Under inflammatory conditions, autophagy eliminates damaged organelles and ROS accumulated in osteoblasts, reducing the production of pro-inflammatory factors within cells and thereby preserving the normal proliferation and osteogenic differentiation capacity of these cells (26). By contrast, excessive or insufficient autophagy exerts adverse effects on osteoblasts, persistent inflammation may induce excessive autophagy in osteoblasts, leading to apoptosis and further impairing osteogenic function (27); meanwhile, inadequate autophagy results in the accumulation of cellular waste, which hinders the synthesis and secretion of osteogenesis-related proteins such as OCN (28). Additionally, autophagy activation can promote the differentiation of BMSCs into mature osteoblasts by upregulating the expression of osteogenic markers including Runx2 and OCN (29).

Therefore, the present study aimed to explore the potential of BA in treating bone loss in OVX rats and investigate the role of osteoblast inflammatory injury in OP and further confirm whether BA can exert a protective effect on OB by inducing autophagy and inhibiting NLRP3-induced inflammatory injury.

Materials and methods

Reagents and antibodies. BA, 3-Methyladenin (3-MA), ROS scavenger N-acetyl-L-cysteine (NAC), NLRP3 inhibitor MCC950 and Dorsomorphin (synonyms: Compound c, CC) were purchased from MedChemExpress, and Essential Medium α (α-MEM) and fetal bovine serum (FBS) were purchased from Gibco, Thermo Fisher Scientific, Inc. The primary antibodies against NLRP3 (cat. no. BF8029), Asc (cat. no. DF6304), Caspase-1 (cat. no. AF5418), Cleaved Caspase-1 (cat. no. AF4005), IL-1β (cat. no. BF8021), AMPK (cat. no. AF6423), phosphorylated (p-)AMPK (cat. no. AF3423), mTOR and p-mTOR were obtained from Affinity Biosciences. The primary antibodies for LC3b (cat. no. ab192890), Beclin-1 (cat. no. ab207612), P62 (cat. no. ab109012), OPN (cat. no. ab283656) and RUNX2 (cat. no. ab192256) were purchased from Abcam.

Cell cultures and drug treatments. MC3T3-E1 cells, derived from mouse calvarial pre-osteoblasts, were purchased from Procell Life Science & Technology Co., Ltd. (cat. no. CRL-2593). The cells were seeded in 6-well plates containing α-MEM, 10% FBS, 100 IU/ml penicillin and 100 μg/ml streptomycin. After 24 h, the old medium was discarded and replaced with the osteogenic induction and differentiation medium (cat. no. CM-0378; Procell Life Science & Technology Co., Ltd.). The medium was then replaced every 3 days to conduct the induction of osteoblasts. After pretreating MC3T3-E1 cells with different concentrations of BA, the cells were treated with 200 μM H_2O_2 to establish an inflammatory injury cell model. The cells were cultured in a humidified incubator with a moist balanced air containing 5% carbon dioxide at 37˚C.

Cell viability assays. MC3T3-E1 cells were seeded into 96-well plates at a density of $3x10^3$ cells. The cells were then treated with BA at concentrations of 0, 5, 10, 20, 30 and 40 μM, respectively, for 24 and 48 h. Subsequently, the cytotoxicity was evaluated.

The Cell Counting Kit-8 (CCK-8; cat. no. C0037; Beyotime Institute of Biotechnology) detection kit was used to determine cell viability. Briefly, 10 μl CCK-8 was added to each well (100 μl medium), incubated at 37˚C for 1 h, and absorbance was measured. The absorbance value, optical density, was accurately measured at a wavelength of 450 nm using a microplate reader (ELx800; Thermo Fisher Scientific, Inc.).

Alkaline phosphatase (ALP) activity and staining. MC3T3-E1 cells were seeded in 6-well plates. Cells were pretreated with 0, 10, and 20 μM of BA for 24 h. The medium was then replaced with osteogenic differentiation medium, treated with H_2O_2 for 24 h, and cultured for 7 days, with the medium changed every 3 days. After fixing the cell samples, they were washed 3-5 times. The BCIP/NBT (cat. no. C3206; Beyotime Institute of Biotechnology) staining working solution was then added for 30 min in the dark, the color development reaction was then terminated. Cell images were obtained using an optical (bright-field) microscope (Leica Microsystems GmbH).

Alizarin red staining (ARS). MC3T3-E1 cells were seeded in 6-well plates and pretreated with 0, 10, and 20 μM of BA for 24 h. The medium was then replaced with osteogenic differentiation medium containing H_2O_2 and cultured for 14 days. The medium was changed every 3 days. The samples were fixed with 4% paraformaldehyde (PFA) at room temperature for 20 min. The samples were washed three times with PBS and the ARS (cat. no. C0148S; Beyotime Institute of Biotechnology) staining solution was applied for 30 min at room temperature before terminating the reaction. Cell images were obtained using an optical microscope (Leica Microsystems GmbH).

Monodansylcadaverine (MDC) staining. MC3T3-E1 cells were seeded in 96-well plates, treated per experimental protocols, then culture medium was aspirated. 100 μl MDC (cat. no. C3018; Beyotime Institute of Biotechnology) staining solution was added to each well, followed by 30-min light-protected incubation at 37˚C. After discarding the stain, cells were rinsed thrice with Assay Buffer, and green fluorescence was visualized via fluorescence microscopy.

Immunofluorescent staining. MC3T3-E1 cells were plated on coverslips and pretreated with different concentrations of BA. Subsequently, the culture medium was replaced with fresh α-MEM containing 200 μM H_2O_2 and incubated under standard conditions (37˚C; 5% CO_2) for 24 h. Initial fixation was performed with 4% PFA for 15 min. Subsequently, the cells were permeabilized with 0.2% Triton X-100 for 10 min. To minimize non-specific binding, specimens were incubated with Rapid Immunofluorescence Blocking Buffer at room temperature for 30 min. Primary antibody incubation was performed using rabbit anti-LC3b (1:50) overnight at 4˚C, followed by three PBS washes. Secondary antibody incubation was performed using Cy3-labeled goat anti-rabbit IgG (1:200; cat. no. A0507; Beyotime Institute of Biotechnology) at room temperature for 1 h. Nuclear counterstaining was performed with DAPI (5 μg/ml). Cell images were captured using an inverted fluorescence microscope (Leica Microsystems GmbH). Additionally, ImageJ software (v1.53t; National Institutes of Health) was employed to quantitatively analyze the average fluorescence intensity.

Intracellular ROS detection. Intracellular ROS generation was assessed using 2',7' dichloro-dihydro-fluorescein diacetate (DCFH-DA; cat. no. S0034; Beyotime Institute of Biotechnology). MC3T3-E1 cells were plated in 96-well culture plates at $3x10^3$ cells/well. Cells were then pretreated with 0, 10, and 20 μM of BA for 24 h. The medium was then replaced with fresh medium containing H_2O_2 and culture for 24 h. Prior to analysis, cells were loaded with 10 μM DCFH-DA in serum-free medium (37˚C; 30 min) and immediately image was captured using an inverted fluorescence microscope (Leica Microsystems GmbH).

Western blot analysis. After treating the cells under the aforementioned conditions, the cells were lysed using a buffer containing RIPA (cat. no. P0013; Beyotime Institute of Biotechnology), PMSF (cat. no. ST505; Beyotime Institute of Biotechnology) and phosphatase inhibitors (cat. no. P1081; Beyotime Institute of Biotechnology) to extract the total cellular proteins. According to the manufacturer's instructions, a BCA assay kit was used to determine the protein concentration. Subsequently, the proteins in the samples were separated using 10% SDS-polyacrylamide gels (loading: 30 μg per lane) and an electrophoresis apparatus. The proteins then were transferred onto a PVDF membrane. After blocking the membrane with a rapid protein-free blocking solution at room temperature for 30 min, the membrane was probed with the primary antibody overnight at 4˚C. After that, the membrane was rinsed three times with Tris-buffered saline containing 0.1% Tween 20 and then incubated with the corresponding secondary antibody (1:1,000; cat. no. A0208 or A0192; Beyotime Institute of Biotechnology) at room temperature for 2 h. Finally, protein expression was detected using an enhanced chemiluminescence reagent (cat. no. MI00607B; Mouse Biotech), and its intensity was analyzed using ImageJ software.

Reverse transcription-quantitative polymerase chain reaction (RT-qPCR). Total RNA was isolated from MC3T3-E1 cells using TRIzol™ Reagent (Thermo Fisher Scientific, Inc.) following the manufacturer's protocol. For RT, RNA (1 μg) was combined with oligo (dT) primers (10 μM) and deoxyribonucleoside triphosphates (dNTPs; 10 mM) in a 20 μl reaction volume. The reverse transcription reaction was carried out at 42˚C for 60 min, followed by 85˚C for 5 min to inactivate the reverse transcriptase. Primers employed for amplification are shown in Table I. The obtained complementary DNA (cDNA) was used as a template to determine the gene expression levels on the LightCycler® 96 system using SYBR Green I (Thermo Fisher Scientific, Inc.) as the fluorophore. The reaction conditions of PCR amplification were as follows: Denaturation at 95˚C for 10 min and followed by 40 cycles at 95˚C for 15 sec, then decreased to 60˚C for 15 sec and finally increased to 72˚C for 40 sec. Relative gene expression levels were calculated using the $2^{-\Delta\Delta Cq}$ method (30).

Animals and treatment. All animal experimental protocols were examined and approved by the Laboratory Animal Management Committee of Xi'an Jiaotong University (approval no. XJTUAE2025-3812). Animals were housed under controlled conditions (22±2˚C, 50±10% humidity, 12/12-h light/dark cycle) with free access to food and water and were implemented following the Xi'an Jiaotong University Guide for Animal Experimentation, which conforms to the requirements of the Guide for the Care and Use of Laboratory Animals issued by the US National Institutes of Health. A total of 30 Sprague-Dawley female rats (8-weeks-old; weight, 180±10 g) were acquired from Xi'an Jiaotong University.

Table I. Primer sequences used for reverse transcription-quantitative PCR analysis.

Gene name	Primer sequence (5'-3')
Runt-related transcription factor 2	Forward: CCGCACGACAACCGCACCAT
	Reverse: CGCTCCGGCCCACAAATCTC
OPN	Forward: CGTCCCTACAGTCGATGTCC
	Reverse: TGTGGCATCAGGATACTGTTCA
β-actin	Forward: CCTAGGCACCAGGGTGTGAT
	Reverse: GGTTGGCCTTAGGGTTCAGG

Based on the formula provided by MedChemExpress official guidelines: Animal A (mg/kg)=Animal B (mg/kg) x (Animal A Km/Animal A Km) and the recommended intraperitoneal administration volume range for rats, the *in vivo* regimen was rationally designed. The rats were divided into three groups: Sham + Vehicle, OVX + Vehicle, and OVX + BA (15 mg/kg; n=10) randomly. The three groups of rats were acclimated for 1 week. Before all surgical and sampling procedures, the rats were anesthetized with inhaled isoflurane (4% for induction and 2% for maintenance) to ensure adequate anesthesia. OVX + BA group rats were intraperitoneally administered 15 mg/kg/day BA every other day for 8 weeks. Rats in the sham and OVX + Vehicle groups were intraperitoneally administered with equal volumes of the excipient. After 8 weeks of treatment, blood was collected from the heart of the rats. Then, the rats were euthanized by cervical dislocation. The femurs were removed and fixed with 4% PFA for subsequent experiments.

ELISA detection. Cardiac blood samples were obtained via cardiac puncture and subjected to two-step centrifugation to isolate serum fractions. Serum concentrations of proinflammatory cytokines were quantified using ELISA kits: IL-1β (cat. no. GER008), IL-6 (cat. no. GER011) and TNF-α (cat. no. GER013; all from Elabscience Biotechnology, Inc.), following the manufacturer's protocols.

Micro-CT analyses. The prepared femur samples were placed in a high-resolution Micro-CT scanner (Skyscan 1276; Bruker Corporation). Raw projection data were reconstructed into three-dimensional models through sequential processing with NRecon (v1.7.4.2; Bruker-microCT) and Data Viewer (v1.5.6.2, Bruker-microCT) software packages (Bruker-microCT). Quantitative morphometric analysis within the metaphyseal region of interest included bone mineral density (BMD, mg HA/cm^3), bone volume fraction (BV/TV, %), trabecular number (Tb.N, mm^{-1}) and trabecular separation (Tb.Sp, μm).

H&E, Masson and immunohistochemical (IHC) staining. Femoral specimens were subjected to decalcification in 10% EDTA solution, achieving complete decalcification within 8-week duration. Specimens subsequently underwent graded ethanol dehydration series (70-100%) and paraffin embedding using standard histology protocols. Subsequently, the specimens were cut into thin slices with a thickness of 4 μm. Finally, according to the standard laboratory procedures, the H&E and Masson staining methods were used respectively to stain the slices.

Paraffin sections underwent xylene dewaxing and graded ethanol rehydration. After that, they were subjected to citrate buffer antigen retrieval. Then, 5% bovine serum albumin (cat. no. HY-D0842; MedChemExpress) was used to block the non-specific binding at room temperature for 30 min. Incubation followed successively with the corresponding primary antibody and secondary antibody. Chromogenic development with 3,3'-diaminobenzidine was monitored microscopically until optimal signal intensity, followed by hematoxylin counterstaining (30 sec) and permanent mounting with resinous medium. Brightfield imaging was performed using a microscope. Quantitative histo-morphometric analysis of staining intensity was conducted through ImageJ with IHC Profiler plugin.

mRFP-GFP-LC3 puncta assay. Cells were seeded onto chamber slides and infected using the 1/2 small-volume method with HBAD-mRFP-GFP-LC3 adenovirus (cat. no. HB-AP210000; Hanbio Biotechnology Co., Ltd.) at 500 multiplicity of infection at 37˚C for 24 h. After transfection, the cells were subjected to the designated treatments and then examined under a confocal microscope at 48 h post-infection. Yellow puncta (RFP$^+$GFP$^+$) were identified as autophagosomes, while red puncta (RFP$^+$GFP$^-$) represented autophagolysosomes. Autophagic flux was assessed by manually counting the number of yellow and red puncta in the merged images. Successful transfection efficiency was verified, and representative fluorescence images are shown in Fig. S1.

Statistical analysis. All experimental data were obtained from at least three independent experiments and were expressed as the mean ± SD. Statistical analyses were performed using SPSS 24.0 software (IBM Corp.). Comparisons between two groups were conducted using unpaired Student's t-test, and Cohen's d was calculated to estimate effect size. For comparisons among multiple groups, one-way analysis of variance (ANOVA) followed by Tukey's post hoc test was applied. When appropriate, 95% confidence intervals (95% CI) were provided for key outcome measures. $P<0.05$ was considered to indicate a statistically significant difference. In addition, post-hoc power analysis was conducted using G*Power 3.1 based on key outcome measures (effect size f=0.32, α=0.05, n=10 per group). $P<0.05$ was considered to indicate a statistically significant difference.

Results

Protective effect of BA on OVX-induced bone loss in rats. To evaluate the *in vivo* safety of BA, (HC staining was carried out

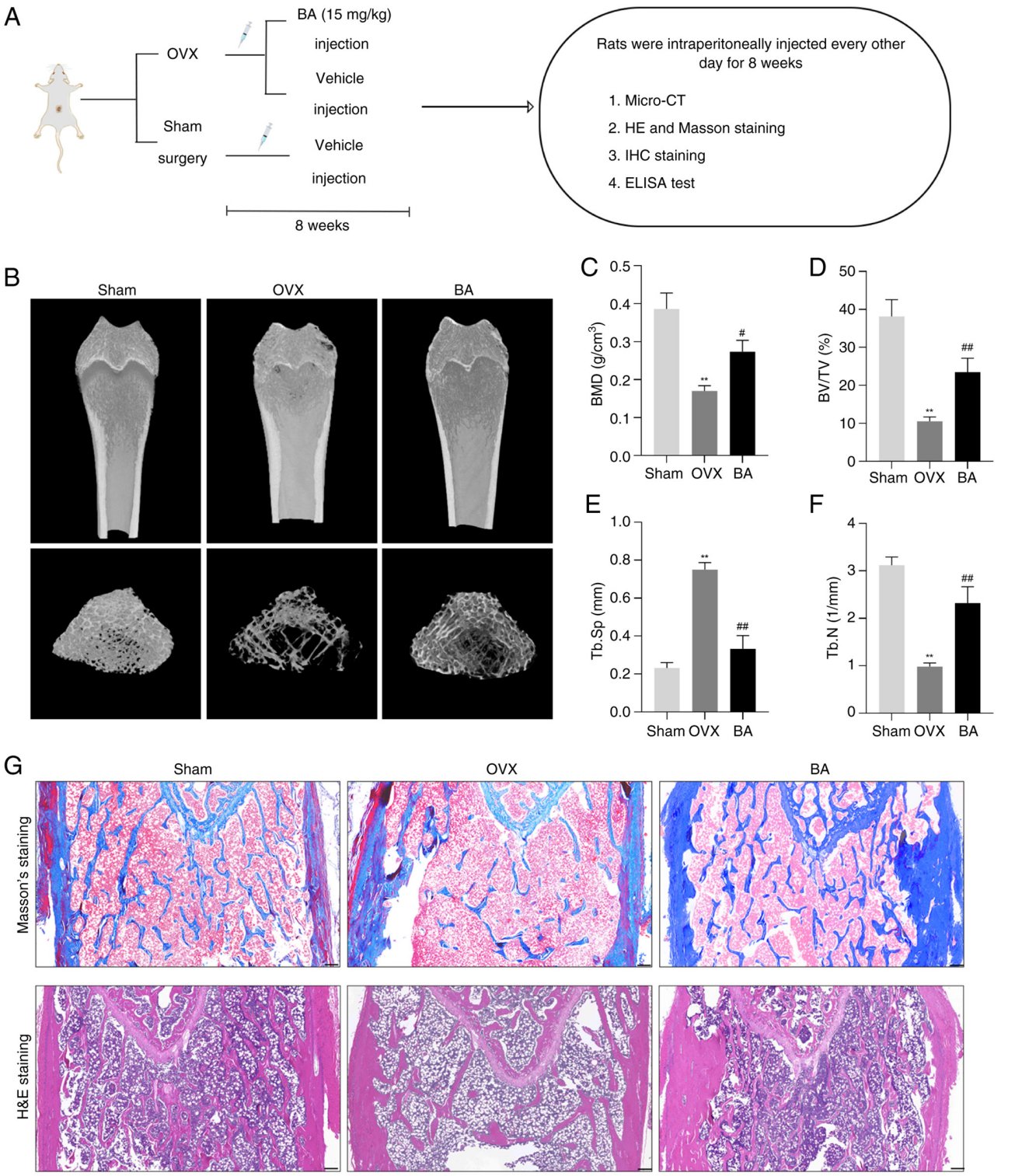

Figure 1. Protective effect of BA on OVX-induced bone loss in rats. (A) Flow chart representing the study design protocol to evaluate the therapeutic effect of BA on OVX rats. (B) Representative images of femurs in each group of rats detected by micro-CT. (C-F) Quantitative analyses of bone structural parameters: BMD, BV/TV, Tb.Sp and Tb.N. (G) Masson's staining and H&E staining of metaphyseal tissue sections of femurs. Scale bar, 200 μm. Data are expressed as the mean ± SEM. **P<0.01 vs. sham group; $^{\#}$P<0.05 and $^{\#\#}$P<0.01 vs. corresponding OVX group. BA, betulinic acid; OVX, ovariectomized; BMD, bone mineral density; BV/TV, bone volume fraction; Tb.N., trabecular number; Tb.Sp, trabecular separation; IHC, immunohistochemical.

on major organs (liver, heart, lung and kidney) of Sham, OVX and BA groups (Fig. S2). Histopathological analysis revealed intact tissue structures and no obvious abnormalities (such as inflammatory infiltration, necrosis or structural damage) in the major organs of the BA groups. No significant histological differences were observed among the three groups, preliminarily confirming the favorable *in vivo* safety of BA at the experimental dose in OVX rats. To explore the effect of BA on bone loss in OVX rats, focus was addressed on the rat femurs (Fig. 1A). The micro-CT images and bone parameters of the rat femurs were analyzed. In addition, the changes in the microstructure of the rat bone tissue were evaluated by

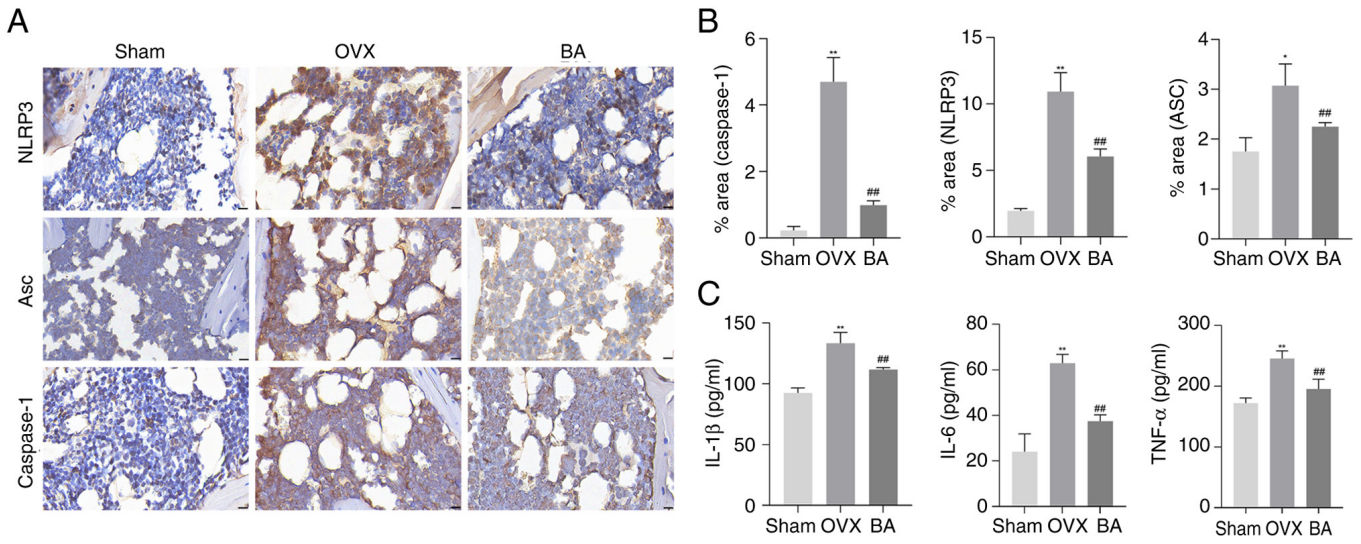

Figure 2. Protective effect of BA on OVX-induced inflammation in rats. (A) Immunohistochemical analysis was performed to detect the expression of NLRP3, Asc and Caspase 1 in rat femoral epiphyseal tissue. Scale bar, 100 μm. (B) Positive areas of NLRP3, Asc and Caspase 1 in rat femoral epiphyseal tissue. (C) The expression levels of IL-1β, IL-6 and TNF-α in rat serum. Data are expressed as the mean ± SEM. *P<0.05 and **P<0.01 vs. sham group; $^{\#\#}$P<0.01 vs. corresponding OVX group. BA, betulinic acid; OVX, ovariectomized; NLRP3, NOD-like receptor pyrin domain-containing 3.

Masson's trichrome staining and H&E staining. The results of the CT scan showed that, compared with the OVX group, the BMD, BV/TV and Tb.N in the BA group were significantly higher, whereas Tb.Sp was significantly lower. (Fig. 1B-F). The results of Masson's trichrome staining revealed that, compared with the OVX group, the BA group significantly increased the generation of bone collagen fibers (Fig. 1G). The results of H&E staining demonstrated that, compared with the OVX group, the BA group alleviated the manifestations of trabecular bone reduction and fracture (Fig. 1G). Post-hoc power analysis indicated that the current sample size (10 rats per group) achieved 83.6% power for one-way ANOVA, confirming the reliability of these primary outcome measures. These findings indicate that BA can prevent OVX-induced bone loss.

Protective effect of BA on OVX-induced inflammation in rats. To further investigate the mechanism by which BA prevents bone loss in OVX rats, the expression levels of NLRP3, Asc and Caspase-1 protein in the femoral tissues of the rats were assessed through IHC staining. Additionally, ELISA was used to detect the inflammatory markers IL-1β, IL-6 and TNF-α in the rat serum. IHC staining of the femurs of OVX rats identified that, compared with the sham group, there was a significant increase in the expression levels of NLRP3, Asc and Caspase-1 protein. However, administration of BA significantly reduced the expression of these inflammation-related proteins (Fig. 2A and B). In addition, the results of ELISA showed that BA could significantly reduce the elevated inflammatory indices of IL-1β, IL-6 and TNF-α in the serum of OVX rats (Fig. 2C). Therefore, these data suggest that BA treatment for bone loss in OVX rats may be associated with its inhibition of the NLRP3 inflammatory pathway in the rat bone tissue.

H_2O_2-induced osteogenic differentiation decline in MC3T3-E1 cells associated with ROS/NLRP3. To further explore the potential of BA treatment and prevention of OP, MC3T3-E1 cells were challenged with H_2O_2 (200 μM) and an inflammatory injury cell model was established *in vitro*. The experimental results showed that, compared with the con group, H_2O_2 intervention significantly increased ROS production in MC3T3-E1 cells (Fig. 3A and B), and the protein expression level of the NLRP3 inflammasome increased (Fig. 3C and D). In addition, as osteogenic differentiation marker factors, both the mRNA and protein expression levels of RUNX2 and OPN were inhibited (Fig. 3E-I). When NLRP3 inhibition experiments were conducted using MCC950 (NLRP3-specific inhibitor) in MC3T3-E1 cells with inflammatory injury, relative to the H_2O_2 group, the expression level of NLRP3 protein decreased significantly (Fig. 3C and D). Moreover, relative to the H_2O_2 group, it significantly improved the expression of RUNX2 and OPN genes and proteins (Fig. 3E-I). Additionally, when NAC (specific ROS inhibitor) was added, in comparison with the H_2O_2 group, the accumulation of ROS was reduced, the expression of NLRP3 protein in the inflammasome was inhibited (Fig. 3A-D), and the inhibition of RUNX2 and OPN gene and protein expression was alleviated (Fig. 3E-I). The aforementioned findings indicate that the effect of H_2O_2 on the osteogenic differentiation of MC3T3-E1 is associated with ROS/NLRP3 inflammasome.

BA attenuates NLRP3-induced inflammatory injury and osteogenic differentiation decline in H_2O_2-exposed MC3T3-E1 cells. Before evaluating the effect of BA (Fig. 4A) on the differentiation of MC3T3-E1 cells treated with H_2O_2, the CCK-8 activity assay was used to detect whether there were potential cytotoxic effects on MC3T3-E1 cells within 24 and 48 h. When the concentration of BA ≤20 μM, there was no significant change in cell viability (Fig. 4B). Consistent with previous studies reporting that BA shows no cytotoxicity to osteoblast-lineage cells within the range of 0-30 μM (31), 10 and 20 μM were therefore selected for subsequent experiments. MC3T3-E1 cells were treated with BA at different concentrations. The results showed that BA (20 μM) significantly inhibited the activation of the NLRP3

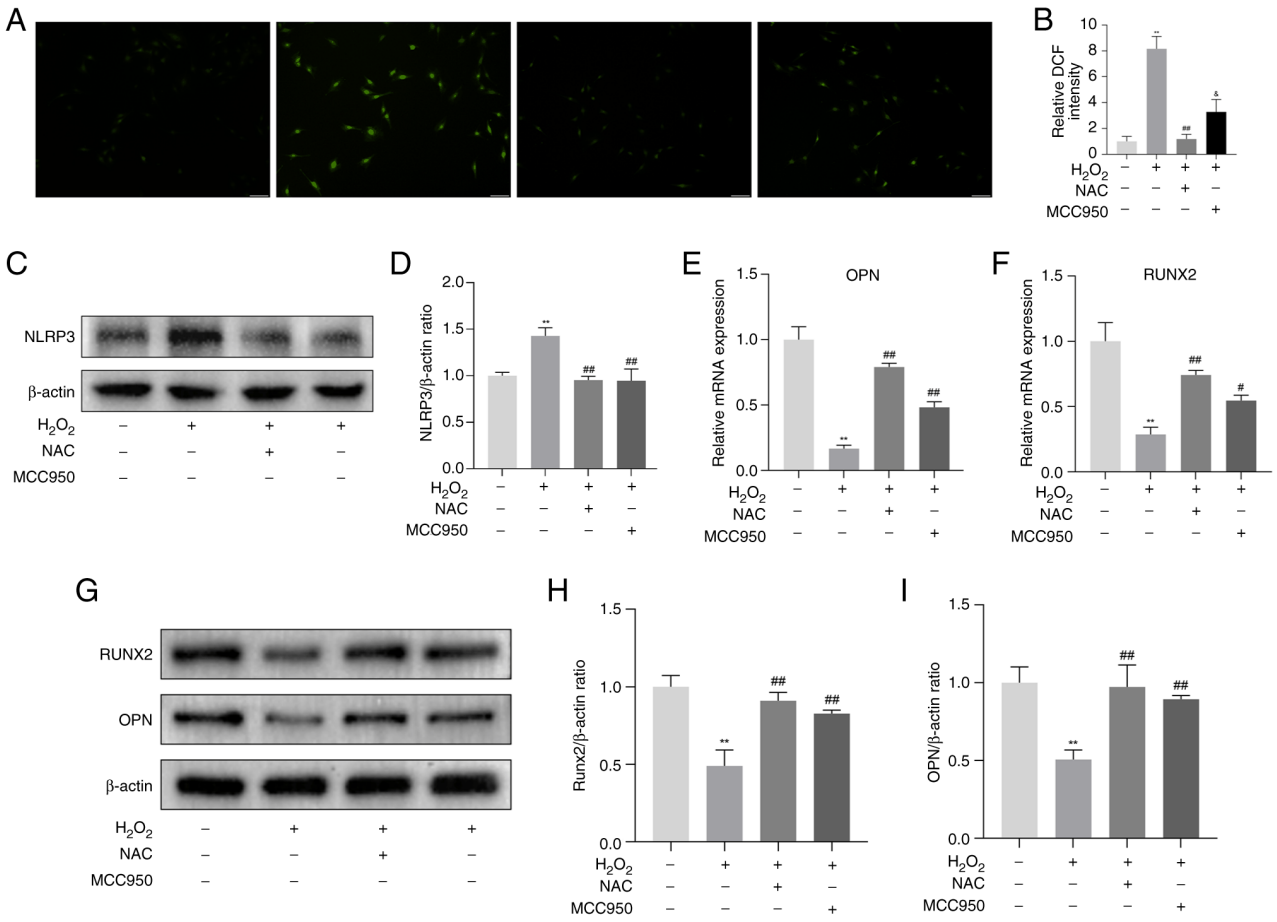

Figure 3. H_2O_2-induced osteogenic differentiation decline in MC3T3-E1 cells related to ROS/NLRP3. (A) MC3T3-E1 was cultured with ROS inhibitor NAC (20 μM) or NLRP3 inhibitor MCC950 (100 μM) in a medium containing H_2O_2 (200 μM) to produce ROS, and then intracellular ROS was detected by DCFH-DA. Scale bar, 100 μm. (B) The average relative DCF fluorescence intensity on each pore cell was evaluated and quantified. (C) The protein levels of NLRP3 were determined by western blotting. (D) Quantification of the results shown in C. (E and F) Quantitative analysis of the expression of osteoblast marker mRNA in osteoblasts treated with NAC or MCC950 with or without H_2O_2 by reverse transcription-quantitative PCR. (G) The protein levels of related markers in the process of osteoblast induction were determined by western blotting. (H and I) Quantification of the results shown in G. Data are expressed as the mean ± SEM. **P<0.01 vs. control group; $^{\#}$P<0.05 and $^{\#\#}$P<0.01 vs. corresponding H_2O_2 group; $^{\&}$P<0.01 vs. corresponding H_2O_2 group. ROS, reactive oxygen species; NAC, N-acetyl-L-cysteine; NLRP3, NOD-like receptor pyrin domain-containing 3; RUNX2, runt-related transcription factor 2.

inflammasome pathway induced by H_2O_2 (Fig. 4C-H). In addition, the results of ARS and ALP staining revealed that, BA (20 μM) significantly restored the activity of ALP and the number of mineralized nodules (Fig. 4I). Similarly, by detecting the mRNA expression of RUNX2 and OPN, it was found that when treated with BA (20 μM), the mRNA expression of the two was significantly restored (Fig. 4J-K). These results demonstrate that BA can effectively treat H_2O_2-induced inflammatory damage and significantly alleviate the inhibitory effect of H_2O_2 on osteoblast differentiation.

BA enhances autophagy in H_2O_2-exposed MC3T3-E1 cells. Based on the previous experimental data, 20 μM was determined as the optimal concentration for BA. To explore the effect of BA on autophagy in MC3T3-E1 cells treated with H_2O_2, the expression of autophagy marker proteins was detected. The results showed that BA significantly increased the expression of LC3b II and Beclin-1 in the cells and inhibited the expression of P62. However, 3-MA could reverse the effects of BA on the expression of LC3b-II, Beclin-1 and P62 (Fig. 5A-D). Immunofluorescence results showed that, compared with the control group, the expression of LC3b in cells increased significantly, and the 3-MA group reversed this result (Fig. 5E and F). MDC can specifically label autophagosomes. MDC staining showed that BA can promote the formation of autophagosomes (Fig. 5G and H). The fluorescent probe DCFH-DA was used to detect intracellular ROS. The BA group significantly inhibited the production of ROS, but the 3-MA group reversed this result (Fig. 5I). Additionally, based on the mRFP-GFP-LC3 puncta assay, the autophagic flux was dynamically evaluated under different conditions. In the BA treatment group, there was a marked increase in both yellow puncta (autophagosomes) and red puncta (autolysosomes), indicating that BA significantly promoted autophagosome formation and enhanced autophagic flux. By contrast, when bafilomycin A1 was added together with BA, yellow puncta remained abundant, but red puncta were markedly reduced. This suggests that although autophagosome formation was still induced, the fusion and degradation steps were blocked, leading to autophagosome accumulation. These findings demonstrate that BA enhances autophagy by promoting autophagic flux (Fig. S3). This indicates that BA can enhance autophagy and inhibit ROS production in H_2O_2-exposed MC3T3-E1 cells.

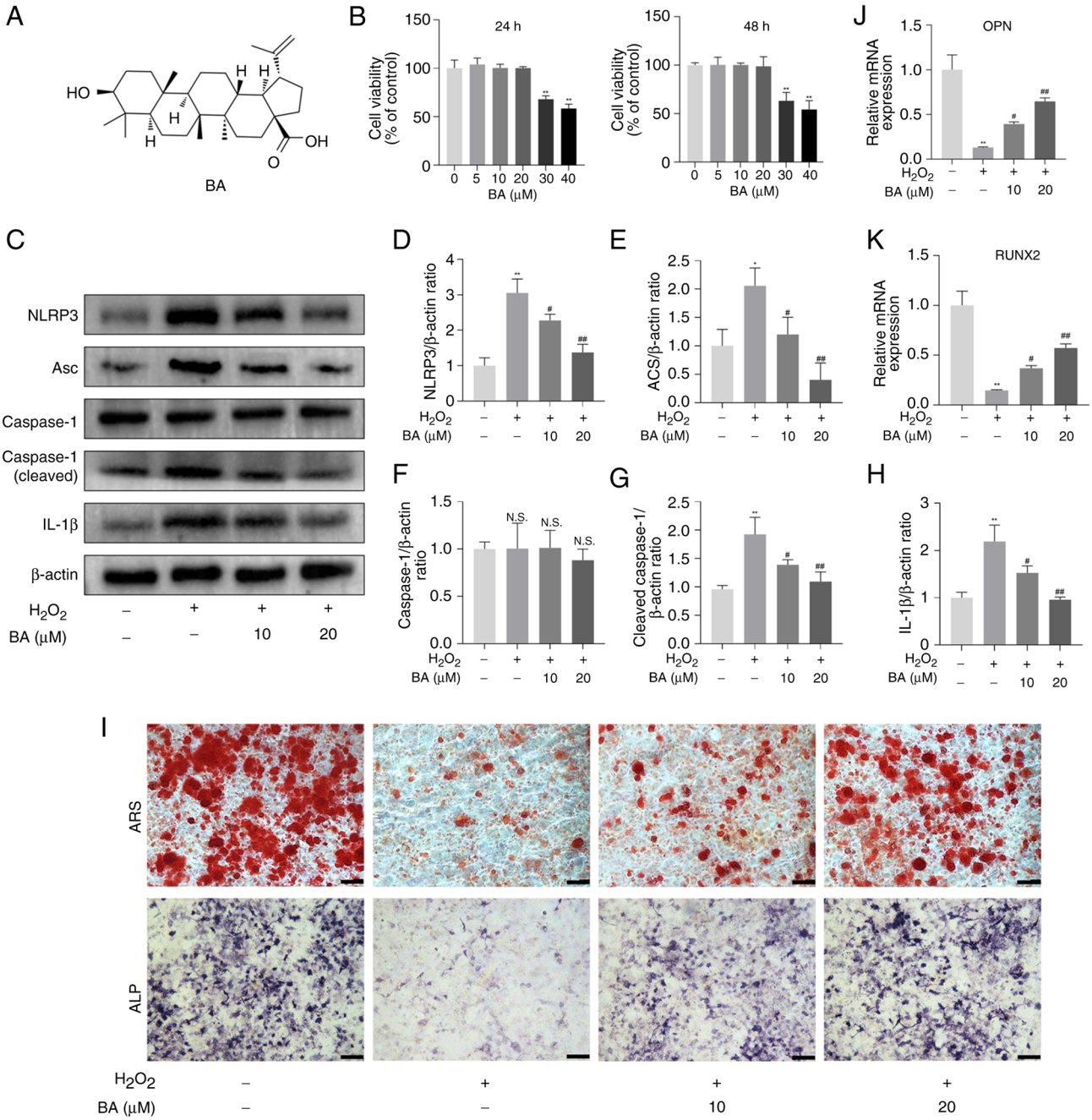

Figure 4. BA attenuates NLRP3-induced inflammatory injury and osteogenic differentiation decline in H_2O_2-exposed MC3T3-E1 cells. (A) The chemical structure of BA. (B) MC3T3-E1 cells were treated with different concentrations of BA (0, 5, 10, 20, 30 and 40 μM) for 24 and 48 h. Cell viability was measured by Cell Counting Kit-8 assay. (C) MC3T3-E1 cells were incubated in the presence of H_2O_2 (200 μM) medium with the BA (10 μM) or BA (20 μM), western blot analysis was performed against NLRP3, Asc, caspase-1, cleaved caspase-1 and IL-1β. (D-H) Quantification of the results shown in C. (I) ALP and ARS staining were performed in MC3T3-E1 cells. (J and K) Quantitative analysis of osteoblast marker gene expression after treatment with different concentrations of BA using reverse transcription-quantitative PCR. Data are expressed as the mean ± SEM. **P<0.01 vs. control group; $^{\#}$P<0.05 and $^{\#\#}$P<0.01 vs. corresponding H_2O_2 group. BA, betulinic acid; NLRP3, NOD-like receptor pyrin domain-containing 3; ALP, alkaline phosphatase; ARS, alizarin red staining; RUNX2, runt-related transcription factor 2; N.S., not significant.

BA activates the AMPK/mTOR signaling pathway in H_2O_2-exposed MC3T3-E1 cells. The regulation of autophagy by BA was investigated. It has been reported that BA can regulate AMPK phosphorylation (32). Western blotting showed that BA effectively promoted the phosphorylation of AMPK and inhibited the phosphorylation of mTOR, while compound C (an AMPK blocker) significantly reversed this effect and inhibited the expression of LC3b-II and Beclin-1, promoting the expression of P62 (Fig. 6A-G). The group treated with compound C also inhibited the expression of LC3b as detected by immunofluorescence and the formation of autophagosomes as shown by MDC staining (Fig. 6H-K). This indicates that BA regulates autophagy in H_2O_2-exposed MC3T3-E1 cells through the AMPK/mTOR pathway.

Discussion

In humans, bones are constantly in a continuous remodeling cycle. Under physiological conditions, mesenchymal-derived osteoblasts and hematopoietic-derived osteoclasts maintain

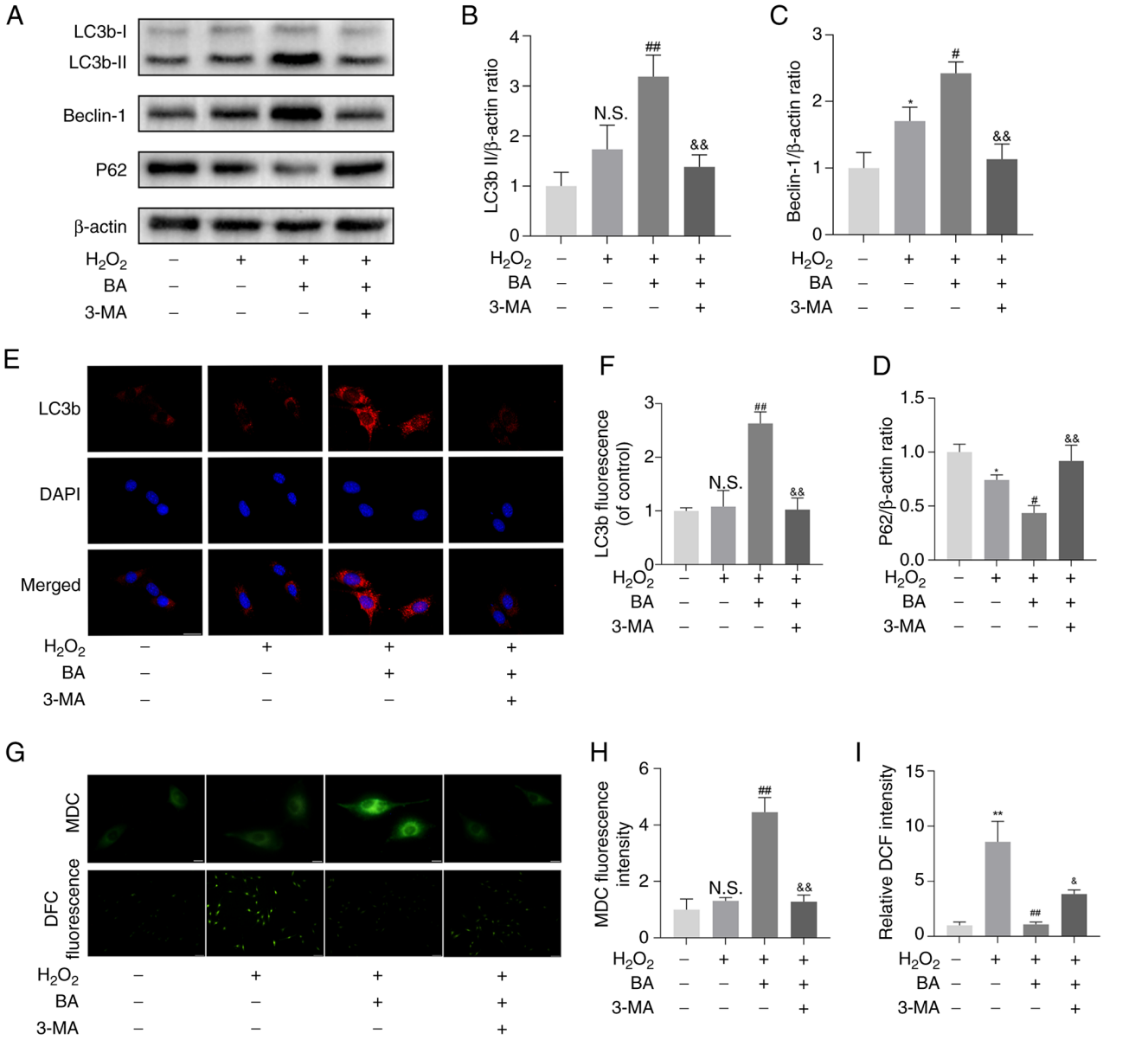

Figure 5. BA enhances autophagy in H_2O_2-exposed MC3T3-E1 cells. (A) MC3T3-E1 cells were incubated in the presence of H_2O_2 (200 μM) medium with the BA (20 μM) or BA (20 μM) + 3-MA, western blot analysis was performed against LC3b, beclin-1 and p62. (B-D) Quantification of the results shown in A. (E) The expression of lc3b protein was detected by immunofluorescence. (F) Quantification of the results shown in E. (G) MDC detected the production of autophagosomes. Intracellular reactive oxygen species were detected by DCFH-DA. (H and I) Quantification of the results shown in G. Data are expressed as the mean ± SEM. *P<0.05 and **P<0.01 vs. control group; $^{\#}$P<0.05 and $^{\#\#}$P<0.01 vs. corresponding H_2O_2 group; $^{\&}$P<0.05 and $^{\&\&}$P<0.01 vs. corresponding H_2O_2 + BA group. BA, betulinic acid; MDC, monodansylcadaverine; 3-MA, 3-methyladenin; N.S., not significant.

the structural stability of bone tissue through synergistic actions (33). The former constructs the bone matrix by synthesizing collagen fibers and inorganic salts, while the latter decomposes the aged bone tissue by acidifying the microenvironment. These two populations of cells with antagonistic functions form a sophisticated functional coupling system under the regulation of cytokines, jointly determining the quality of bone tissue and metabolic homeostasis. When there is a dysfunction in this regulatory network, metabolic imbalance will cause the rate of bone resorption to exceed the bone formation capacity, thus leading to a progressive decrease in bone mineral density and manifestations of OP (34,35).

Studies on the molecular mechanisms of bone metabolism regulation have shown that fluctuations in endogenous hormone levels play an important regulatory role in bone homeostasis (36). Previous studies have confirmed that a decrease in estrogen levels can induce a chronic inflammatory response through the amplifying effect of the NF-κB signaling cascade (37,38). This molecular cascade can severely disrupt the dynamic balance between bone formation and bone resorption, and it is a key pathogenic factor for postmenopausal OP. The regulation of osteogenic differentiation relies on the synergistic action of core signaling pathways, such as the Wnt/β-catenin and BMP/Smad pathways. These pathways drive the differentiation of MSCs into mature osteoblasts and facilitate bone matrix mineralization by activating key transcription factors, including RUNX2 and osterix (39-41). Notably, the inflammatory microenvironment can inhibit osteogenic differentiation by interfering with the aforementioned pathways, such as suppressing Wnt signaling and

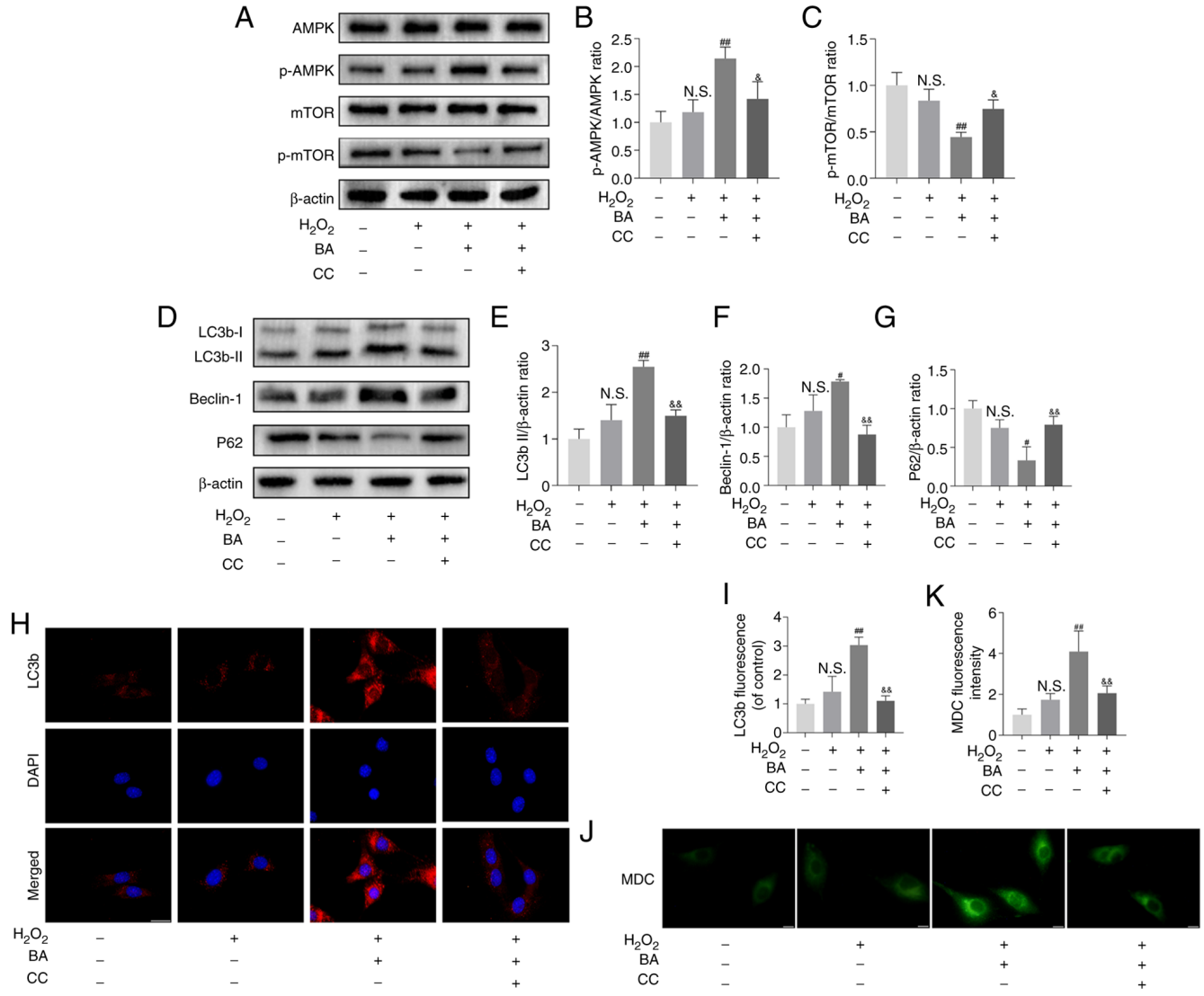

Figure 6. BA activates the AMPK/mTOR signaling pathway in H_2O_2-exposed MC3T3-E1 cells. (A) MC3T3-E1 cells were incubated in the presence of H_2O_2 (200 μM) medium with the BA (20 μM) or BA (20 μM) + CC (AMPK inhibitor), western blot analysis was performed against p-AMPK and AMPK, p-mTOR and mTOR. (B and C) Quantification of the results shown in A. (D) Western blot analysis was performed against LC3b, beclin-1 and p62. (E-G) Quantification of the results shown in D. (H) The expression of lc3b protein was detected by immunofluorescence. (I) Quantification of the results shown in H. (J) MDC detected the production of autophagosomes. (K) Quantification of the results shown in J. Data are expressed as the mean ± SEM. $^{\#}$P<0.05 and $^{\#\#}$P<0.01 vs. corresponding H_2O_2 group; $^{\&}$P<0.05 and $^{\&\&}$P<0.01 vs. corresponding H_2O_2 + BA group. BA, betulinic acid; CC, compound c; p-, phosphorylated; MDC, monodansylcadaverine; N.S., not significant.

abnormally activating Notch signaling (42,43). The positive feedback loop between the systemic low-grade inflammatory state and the ROS-NLRP3 inflammasome axis serves as the core pathological mechanism through which inflammatory damage compromises osteogenic function in postmenopausal OP (44,45). At the molecular level, pathological processes such as mitochondrial dysfunction can activate the NLRP3 inflammasome via ROS-dependent pathways. Mediated by ASC, this activation triggers Caspase-1 cleavage, which in turn promotes the maturation and release of IL-1β, ultimately impairing osteogenic differentiation capacity (46-48). The present study found that MC3T3-E1 cells intervened with H_2O_2 showed increased production of ROS, excessive activation of the NLRP3 pathway, accompanied by a downregulation of the expression levels of osteogenic markers. This suggests that inflammatory injury is a key regulatory step in the impairment of osteogenic differentiation. It is worth noting that both NAC and MCC950 can inhibit the activation of NLRP3 and effectively restore the osteogenic differentiation ability. Moreover, compared with MCC950, NAC can also inhibit the production of ROS. These findings suggest that targeted regulation of the ROS-NLRP3 signaling axis may provide a new molecular intervention strategy for the treatment of OP.

BA, a natural product of pentacyclic triterpenoids, has become a research hotspot in the field of drug development in recent years due to its multiple biological activity characteristics in metabolic diseases, especially its significant anti-inflammatory and antioxidant abilities (49). However, the protective effect of this compound on osteoblast function and its potential value in the treatment of OP have not been elucidated. According to a previous study, the concentration of pro-inflammatory mediators such as IL-1β and TNF-α in the peripheral blood of rats with OVX model markedly increased (50). The present study revealed that the BA intervention group of OVX

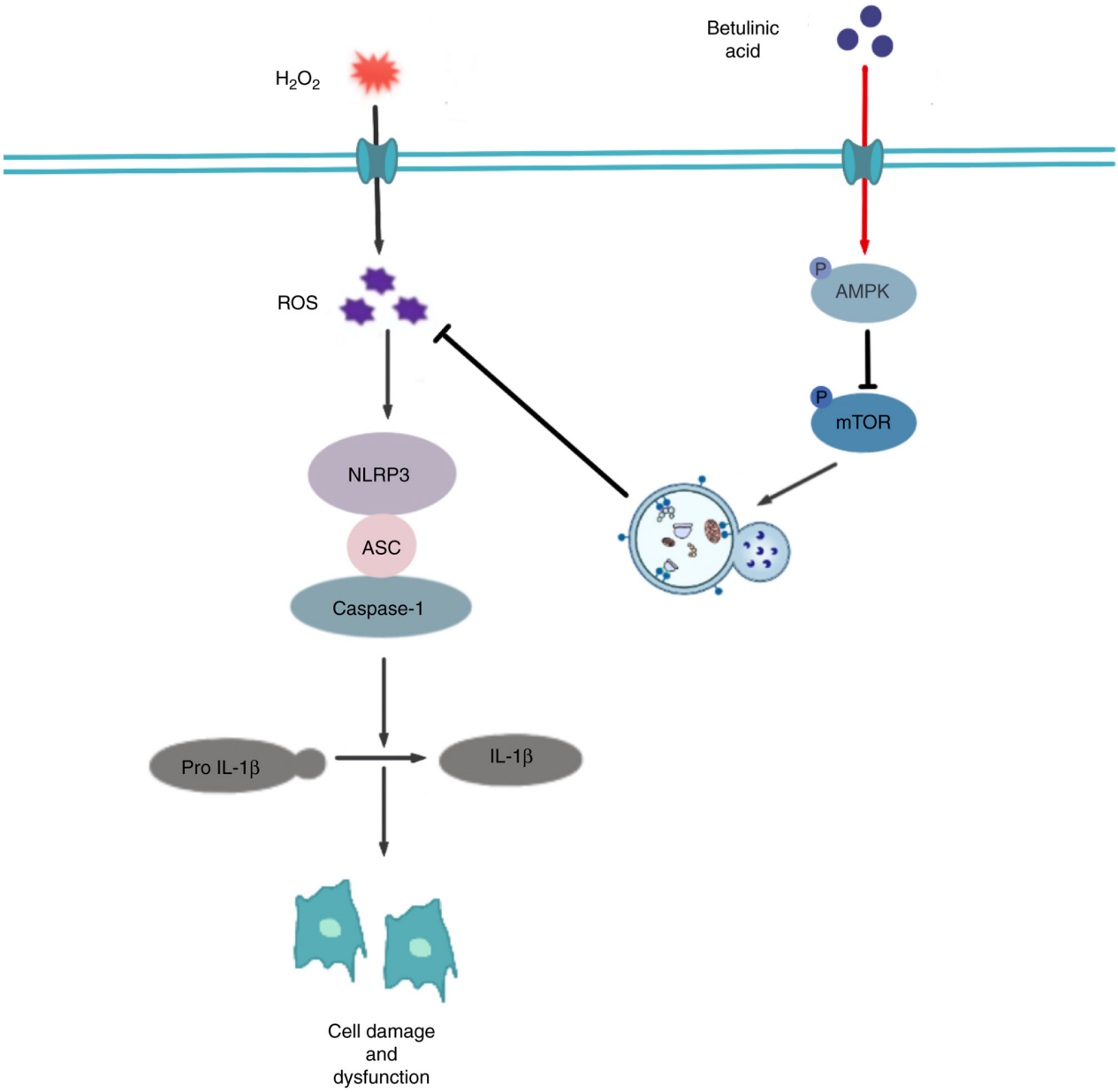

Figure 7. Schematic illustration of the working model demonstrating that betulinic acid activates autophagy via the AMPK/mTOR pathway to inhibit ROS production, thereby suppressing NLRP3 inflammasome activation and alleviating inflammatory damage to osteoblasts. ROS, reactive oxygen species; NLRP3, NOD-like receptor pyrin domain-containing 3.

rats not only significantly reduced the levels of serum inflammatory factors, but also significantly downregulated the protein expression of NLRP3 inflammasome components (NLRP3, Asc and Caspase-1) in their femoral tissue. At the same time, bone microstructural parameters were significantly improved. *In vitro* experiments have confirmed that in MC3T3-E1 cells intervened by H_2O_2, after pretreatment with BA, the NLRP3 inflammasome pathway is inhibited. Meanwhile, the ALP activity of cells is restored, the number of mineralized nodules significantly rebounds, and the inhibited expression of osteoblast-specific genes RUNX2 and OPN is effectively improved. Collectively, these results demonstrate that BA exerts effects in protecting osteoblasts from inflammatory damage, suppressing inflammation in rats, and treating OP in OVX rats. These effects are achieved by inhibition of the activation of the NLRP3 inflammasome by BA.

Autophagy is a key biological activity that responds to various types of stresses and maintains intracellular homeostasis. It can assist cells in processes such as clearing damaged organelles and misfolded proteins, ensuring the stability of the intracellular environment, thereby enabling cells to maintain normal physiological functions in various complex internal and external environmental changes (51). An increasing number of studies have shown that autophagy plays an important role in scavenging ROS and inhibiting the activation of the NLRP3 inflammasome (52,53). Moreover, BA can regulate the autophagy levels of some tissues and cells (18,23,32). Autophagy can be detected by examining the expression levels of common markers such as LC3b-II/I, Beclin-1, and P62. Additionally, the formation of autophagosomes can also be detected by MDC. The present study is the first to demonstrate that, in MC3T3-E1 cells treated with H_2O_2, BA can

promote the expression of LC3b-II and Beclin-1, inhibit the expression of P62, and significantly increase the formation of autophagosomes. In addition, BA can inhibit ROS production through autophagy, and the autophagy inhibitor 3-MA can reverse this effect. These findings indicate that the protective effect of BA against inflammatory injury in MC3T3-E1 cells is partly attributed to the enhancement of autophagy, which reduces ROS production and inhibits the activation of NLRP3. Among a variety of pathways for regulating autophagy, the AMPK/mTOR axis is classical and widely known (54). However, it remains unclear whether BA activates the AMPK/mTOR signaling pathway to regulate autophagy in MC3T3-E1 cells treated with H_2O_2. Findings of the present study revealed that BA could promote the phosphorylation of AMPK and weaken the phosphorylation of mTOR, which subsequently led to the activation of autophagy. Compound C, an AMPK inhibitor, could significantly reverse the effect of BA in promoting the phosphorylation of AMPK. These results indicated that the autophagy induced by BA is mediated through the AMPK/mTOR signaling pathway.

In conclusion, the present study demonstrated for the first time that BA may alleviate the chronic low-grade inflammation and OP caused by estrogen deficiency in OVX rats. *In vitro*, the potential mechanism by which BA exerts its effects may be through activating the AMPK/mTOR pathway, promoting cellular autophagy, reducing the excessive production of ROS, thereby decreasing the generation and activation of the NLRP3 inflammasome, maintaining the stability of the intracellular environment, and ensuring the normal differentiation and functions of osteoblasts (Fig. 7). However, the present study also has some limitations. Firstly, pharmacokinetic properties, bioavailability and tissue distribution of BA were not addressed, and the 15 mg/kg dosing regimen in rats was based on recommended guidelines rather than detailed pharmacokinetic modeling. Secondly, previous studies have shown that BA inhibits the generation and differentiation of osteoclasts caused by ROS and inflammation (55,56). However, further investigation is needed to determine whether these regulate autophagy through BA. Thirdly, further research is needed on the safety of BA *in vivo*. Finally, future studies will incorporate positive control groups, such as rapamycin as an autophagy inducer or MCC950 as an NLRP3 inhibitor, to directly compare the efficacy of BA with established therapeutic agents and further clarify its mechanism of action. In summary, the results of the present study indicate that BA is a potential drug for treating diseases associated with osteoblast inflammatory injury and provide relevant evidence for this.

Acknowledgements

The authors sincerely appreciate the technical support provided by the Translational Center Laboratory Platform and Public Technical Service Platform of the Red Cross Hospital Affiliated to Xi'an Jiaotong University.

Funding

The present study was supported by the National Natural Science Foundation of China (grant no. 82501067), the Plan for Health and Medical Research and Innovation Platforms in Shaanxi (grant no. 2025PT-01), the Medical Research Project of Xi'an Science and Technology Bureau (grant no. 24YXYJ0006) and the Key Project of Natural Science Basic Research Plan of Shaanxi (grant no. 2025JC-YBQN-1164).

Availability of data and materials

The data generated in the present study may be requested from the corresponding author.

Authors' contributions

YiZ and ZQ conceptualized and designed the study, analyzed and interpreted the data. YiZ and LY designed the study, drafted the manuscript and carried out the experiments. ZQ, YG and LY revised the manuscript critically for important intellectual content and provided final approval of the version to be published. XW, YoZ, LL and BZ analyzed and interpretated the data. YG, LL, YiZ and BZ carried out the experiments and acquired data. LY acquired funding. LY and ZQ confirm the authenticity of all the raw data. All authors read and approved the final version of the manuscript.

Ethics approval and consent to participate

All animal care and experimental procedures were approved (approval no. XJTUAE2025-3812) by Animal Care Committee of Hong-Hui Hospital, Xi'an Jiaotong University College of Medicine (Xi'an, China) and conducted strictly following the institutional guidelines for the care and use of laboratory animals at the Jiaotong University College of Medicine.

Patient consent for publication

Not applicable.

Competing interests

The authors declare that they have no competing interests.

References

1. Fischer V and Haffner-Luntzer M: Interaction between bone and immune cells: Implications for postmenopausal osteoporosis. Semin Cell Dev Biol 123: 14-21, 2022.
2. Ott SM: Osteoporosis treatment: Not easy. Ann Intern Med 176: 278-279, 2023.
3. Adler RA: Osteoporosis treatment: Decreased mortality too? J Clin Endocrinol Metab 108: e48-e49, 2023.
4. Song S, Guo Y, Yang Y and Fu D: Advances in pathogenesis and therapeutic strategies for osteoporosis. Pharmacol Ther 237: 108168, 2022.
5. Adami G, Fassio A, Rossini M, Caimmi C, Giollo A, Orsolini G, Viapiana O and Gatti D: Osteoporosis in rheumatic diseases. Int J Mol Sci 20: 5867, 2019.
6. Valero C and González Macías J: Atherosclerosis, vascular calcification and osteoporosis. Med Clin (Barc) 164: e13-e20, 2025 (In English, Spanish).
7. Weaver CM: Nutrition and bone health. Oral Dis 23: 412-415, 2017.
8. Kimball JS, Johnson JP and Carlson DA: Oxidative stress and osteoporosis. J Bone Joint Surg Am 103: 1451-1461, 2021.
9. Yao Y, Cai X, Chen Y, Zhang M and Zheng C: Estrogen deficiency-mediated osteoimmunity in postmenopausal osteoporosis. Med Res Rev 45: 561-575, 2025.

10. Zhang YW, Cao MM, Li YJ, Lu PP, Dai GC, Zhang M, Wang H and Rui YF: Fecal microbiota transplantation ameliorates bone loss in mice with ovariectomy-induced osteoporosis via modulating gut microbiota and metabolic function. J Orthop Translat 37: 46-60, 2022.
11. Wang G, Tan J, Huang C, Xu Y, Yang Z and Huo L: Based on NF-κB and Notch1/Hes1 signaling pathways, the mechanism of artesunate on inflammation in osteoporosis in ovariectomized rats was investigated. Front Biosci (Landmark Ed) 29: 266, 2024.
12. Sun D, Peng Y, Ge S and Fu Q: USP1 inhibits NF-κB/NLRP3 induced pyroptosis through TRAF6 in osteoblastic MC3T3-E1 cells. J Musculoskelet Neuronal Interact 22: 536-545, 2022.
13. Xu L, Zhang L, Wang Z, Li C, Li S, Li L, Fan Q and Zheng L: Melatonin suppresses estrogen deficiency-induced osteoporosis and promotes osteoblastogenesis by inactivating the NLRP3 inflammasome. Calcif Tissue Int 103: 400-410, 2018.
14. An T, Zha W and Zi J: Biotechnological production of betulinic acid and derivatives and their applications. Appl Microbiol Biotechnol 104: 3339-3348, 2020.
15. Lou H, Li H, Zhang S, Lu H and Chen Q: A review on preparation of betulinic acid and its biological activities. Molecules 26: 5583, 2021.
16. Zheng X, Cao Z, Wang M, Yuan R, Han Y, Li A and Wang X: Betulinic acid reduces intestinal inflammation and enhances intestinal tight junctions by modulating the PPAR-γ/NF-κB signaling pathway in intestinal cells and organoids. Nutrients 17: 2052, 2025.
17. Xia G, Shen C, Xiao Y, Wang X, Qiu L, Lei S and Jiang R: Shenling Baizhu Powder and Betulin attenuate sepsis-induced intestinal injury by targeting GADD45B/TAOK1/p38 MAPK pathway. J Ethnopharmacol 353: 120282, 2025.
18. Zheng LY, Zou X, Wang YL, Zou M, Ma F, Wang N, Li JW, Wang MS, Hung HY and Wang Q: Betulinic acid-nucleoside hybrid prevents acute alcohol-induced liver damage by promoting anti-oxidative stress and autophagy. Eur J Pharmacol 914: 174686, 2022.
19. Ou Z, Zhu L, Huang C, Ma C, Kong L, Lin X, Gao X, Huang L, Wen L, Liang Z, *et al*: Betulinic acid attenuates cyclophosphamide-induced intestinal mucosa injury by inhibiting the NF-κB/MAPK signalling pathways and activating the Nrf2 signalling pathway. Ecotoxicol Environ Saf 225: 112746, 2021.
20. Li J, Bao G, ALyafeai E, Ding J, Li S, Sheng S, Shen Z, Jia Z, Lin C, Zhang C, *et al*: Betulinic acid enhances the viability of random-pattern skin flaps by activating autophagy. Front Pharmacol 10: 1017, 2019.
21. Liu Y, Bi Y, Mo C, Zeng T, Huang S, Gao L, Sun X and Lv Z: Betulinic acid attenuates liver fibrosis by inducing autophagy via the mitogen-activated protein kinase/extracellular signal-regulated kinase pathway. J Nat Med 73: 179-189, 2019.
22. Liu B, Wu Y, Liang T, Zhou Y, Chen G, He J, Ji C, Liu P, Zhang C, Lin J, *et al*: Betulinic acid attenuates osteoarthritis via limiting NLRP3 inflammasome activation to decrease interleukin-1β maturation and secretion. Mediators Inflamm 2023: 3706421, 2023.
23. Wu C, Chen H, Zhuang R, Zhang H, Wang Y, Hu X, Xu Y, Li J, Li Y, Wang X, *et al*: Betulinic acid inhibits pyroptosis in spinal cord injury by augmenting autophagy via the AMPK-mTOR-TFEB signaling pathway. Int J Biol Sci 17: 1138-1152, 2021.
24. Liu T, Wang L, Liang P, Wang X, Liu Y, Cai J, She Y, Wang D, Wang Z, Guo Z, *et al*: USP19 suppresses inflammation and promotes M2-like macrophage polarization by manipulating NLRP3 function via autophagy. Cell Mol Immunol 18: 2431-2442, 2021.
25. Behera J, Ison J, Tyagi A, Mbalaviele G and Tyagi N: Mechanisms of autophagy and mitophagy in skeletal development, diseases and therapeutics. Life Sci 301: 120595, 2022.
26. Wang J, Zhang Y, Cao J, Wang Y, Anwar N, Zhang Z, Zhang D, Ma Y, Xiao Y, Xiao L and Wang X: The role of autophagy in bone metabolism and clinical significance. Autophagy 19: 2409-2427, 2023.
27. Lin Z, Gu Y, Liu Y, Chen Z, Fang S, Wang Z, Liu Z, Lin Q, Hu Y, Jiang N, *et al*: Melatonin attenuates inflammatory bone loss by alleviating mitophagy and lactate production. Apoptosis 30: 1351-1371, 2025.
28. Tang N, Zhao H, Zhang H and Dong Y: Effect of autophagy gene DRAM on proliferation, cell cycle, apoptosis, and autophagy of osteoblast in osteoporosis rats. J Cell Physiol 234: 5023-5032, 2019.
29. Qiao J, Liu A, Sun C and Liu Q: HIF1A overexpression promotes osteoblast differentiation through activation of autophagy to alleviate osteoporosis. Sci Rep 15: 30370, 2025.
30. Livak KJ and Schmittgen TD: Analysis of relative gene expression data using real-time quantitative PCR and the 2(-Delta Delta C(T)) method. Methods 25: 402-408, 2001.
31. Choi H, Jeong BC, Kook MS and Koh JT: Betulinic acid synergically enhances BMP2-induced bone formation via stimulating Smad 1/5/8 and p38 pathways. J Biomed Sci 23: 45, 2016.
32. Zhang Y, He N, Zhou X, Wang F, Cai H, Huang SH, Chen X, Hu Z and Jin X: Betulinic acid induces autophagy-dependent apoptosis via Bmi-1/ROS/AMPK-mTOR-ULK1 axis in human bladder cancer cells. Aging (Albany NY) 13: 21251-21267, 2021.
33. Wang S, Deng Z, Ma Y, Jin J, Qi F, Li S, Liu C, Lyu FJ and Zheng Q: The role of autophagy and mitophagy in bone metabolic disorders. Int J Biol Sci 16: 2675-2691, 2020.
34. Du J, Wang Y, Wu C, Zhang X, Zhang X and Xu X: Targeting bone homeostasis regulation: Potential of traditional Chinese medicine flavonoids in the treatment of osteoporosis. Front Pharmacol 15: 1361864, 2024.
35. Kim JM, Lin C, Stavre Z, Greenblatt MB and Shim JH: Osteoblast-osteoclast communication and bone homeostasis. Cells 9: 2073, 2020.
36. Li J, Chen X, Lu L and Yu X: The relationship between bone marrow adipose tissue and bone metabolism in postmenopausal osteoporosis. Cytokine Growth Factor Rev 52: 88-98, 2020.
37. Zhang C, Li H, Li J, Hu J, Yang K and Tao L: Oxidative stress: A common pathological state in a high-risk population for osteoporosis. Biomed Pharmacother 163: 114834, 2023.
38. Weitzmann MN and Pacifici R: Estrogen deficiency and bone loss: An inflammatory tale. J Clin Invest 116: 1186-1194, 2006.
39. Cheng CH, Chen LR and Chen KH: Osteoporosis due to hormone imbalance: An overview of the effects of estrogen deficiency and glucocorticoid overuse on bone turnover. Int J Mol Sci 23: 1376, 2022.
40. Wu M, Chen G and Li YP: TGF-β and BMP signaling in osteoblast, skeletal development, and bone formation, homeostasis and disease. Bone Res 4: 16009, 2016.
41. Zanotti S and Canalis E: Notch signaling and the skeleton. Endocr Rev 37: 223-253, 2016.
42. Uluçkan Ö, Jimenez M, Karbach S, Jeschke A, Graña O, Keller J, Busse B, Croxford AL, Finzel S, Koenders M, *et al*: Chronic skin inflammation leads to bone loss by IL-17-mediated inhibition of Wnt signaling in osteoblasts. Sci Transl Med 8: 330ra337, 2016.
43. Zhang H, Hilton MJ, Anolik JH, Welle SL, Zhao C, Yao Z, Li X, Wang Z, Boyce BF and Xing L: NOTCH inhibits osteoblast formation in inflammatory arthritis via noncanonical NF-κB. J Clin Invest 124: 3200-3214, 2014.
44. Livshits G and Kalinkovich A: Targeting chronic inflammation as a potential adjuvant therapy for osteoporosis. Life Sci 306: 120847, 2022.
45. Iantomasi T, Romagnoli C, Palmini G, Donati S, Falsetti I, Miglietta F, Aurilia C, Marini F, Giusti F and Brandi ML: Oxidative stress and inflammation in osteoporosis: Molecular mechanisms involved and the relationship with microRNAs. Int J Mol Sci 24: 3772, 2023.
46. Abais JM, Xia M, Zhang Y, Boini KM and Li PL: Redox regulation of NLRP3 inflammasomes: ROS as trigger or effector? Antioxid Redox Signal 22: 1111-1129, 2015.
47. Que X, Zheng S, Song Q, Pei H and Zhang P: Fantastic voyage: The journey of NLRP3 inflammasome activation. Genes Dis 11: 819-829, 2023.
48. Fu J and Wu H: Structural mechanisms of NLRP3 inflammasome assembly and activation. Annu Rev Immunol 41: 301-316, 2023.
49. Jiang W, Li X, Dong S and Zhou W: Betulinic acid in the treatment of tumour diseases: Application and research progress. Biomed Pharmacother 142: 111990, 2021.
50. Feng R, Wang Q, Yu T, Hu H, Wu G, Duan X, Jiang R, Xu Y and Huang Y: Quercetin ameliorates bone loss in OVX rats by modulating the intestinal flora-SCFAs-inflammatory signaling axis. Int Immunopharmacol 136: 112341, 2024.
51. Liu S, Yao S, Yang H, Liu S and Wang Y: Autophagy: Regulator of cell death. Cell Death Dis 14: 648, 2023.
52. Di Q, Zhao X, Tang H, Li X, Xiao Y, Wu H, Wu Z, Quan J and Chen W: USP22 suppresses the NLRP3 inflammasome by degrading NLRP3 via ATG5-dependent autophagy. Autophagy 19: 873-885, 2023.
53. Lin Q, Li S, Jiang N, Jin H, Shao X, Zhu X, Wu J, Zhang M, Zhang Z, Shen J, *et al*: Inhibiting NLRP3 inflammasome attenuates apoptosis in contrast-induced acute kidney injury through the upregulation of HIF1A and BNIP3-mediated mitophagy. Autophagy 17: 2975-2990, 2021.

54. Chen H, Cheng Y, Du H, Zhang C, Zhou Y, Zhao Z, Li Y, Friedemann T, Mei J, Schröder S, *et al*: Shufeng Jiedu capsule ameliorates olfactory dysfunction via the AMPK/mTOR autophagy pathway in a mouse model of allergic rhinitis. Phytomedicine 107: 154426, 2022.
55. Wei J, Li Y, Liu Q, Lan Y, Wei C, Tian K, Wu L, Lin C, Xu J, Zhao J and Yang Y: Betulinic acid protects from bone loss in ovariectomized mice and suppresses RANKL-associated osteoclastogenesis by inhibiting the MAPK and NFATc1 pathways. Front Pharmacol 11: 1025, 2020.
56. Jeong DH, Kwak SC, Lee MS, Yoon KH, Kim JY and Lee CH: Betulinic acid inhibits RANKL-induced osteoclastogenesis via attenuating Akt, NF-κB, and PLCγ2-Ca^{2+} signaling and prevents inflammatory bone loss. J Nat Prod 83: 1174-1182, 2020.

Copyright © 2026 Zhao et al. This work is licensed under a Creative Commons Attribution-NonCommercial-NoDerivatives 4.0 International (CC BY-NC-ND 4.0) License.